(Received 3 November 2023, Accepted 22 December 2023, Scheduled 1 January 2024)

Hexa-Slot Wheel Shaped Fractal Orthogonal MIMO Antenna with Polarization Diversity for UWB Applications

Ramesh Deshpande[1, 2] and Usha D. Yalavarthi[1, *]

[1] Department of ECE, Koneru Lakshmaiah Education Foundation, AP, India
[2] Department of ECE, B VRaju Institute of Technology, Telangana, India

ABSTRACT: In this paper, a hexa-slot wheel shaped fractal antenna is proposed for UWB applications. Fractal structure (wheel shaped hexa slots) is developed by inscribing hexagons and circles inside a circular patch monopole antenna. Then, orthogonal MIMO antenna with polarization diversity is proposed that operates from 1.39 to 15.18 GHz with an impedance bandwidth of 13.79 GHz. Its performance is analyzed at three resonant frequencies 5.8 GHz, 8.3 GHz, and 10 GHz. It exhibits good diversity performance with ECC < 0.035, DG very close to 10, isolation > 35 dB, CCL < 0.35 bits/s/Hz values. The proposed MIMO fractal antenna achieved an average radiation efficiency of 83.11% with 3.26 dB maximum peak gain. TARC characteristics and time domain behavior using group delay are also examined. Simulated and measured results are in good agreement, and hence the proposed MIMO antenna with polarization diversity is well suitable for UWB applications.

1. INTRODUCTION

The rapid progress in wireless communication technology has made ultrawideband (UWB) a pivotal element in wireless communications. Its ability to offer high data rates, extensive bandwidth, minimal power, and low power made it so significant. Fractal UWB antennas are significant due to their ability to cover a broad frequency range, compact size, omnidirectional radiation, and potential for reducing interference. They find applications in a wide range of fields, including wireless communication, radar systems, medical imaging, environmental monitoring, and asset tracking, among others, making them versatile and valuable components in modern technology. Many researchers have developed [1–22] various fractal antennas and fractal multiple-input multiple-output (MIMO) antennas for UWB applications. A Giusepe Peano and Sierpinski Carpet fractals based UWB monopole antenna with omnidirectional radiation patterns is proposed in [1] with good gain and radiation efficiency. A Pythagorean Tree fractal UWB monopole antenna is developed that operates from 2.6 to 11.12 GHz by the authors in [2]. A Bow-Tie dipole antenna with Koch like sided fractal and a fractal antenna with T-shaped folded elements for UWB applications are presented in [3, 4]. A swastika shaped fractal antenna with an EBG structure, a log periodic UWB antenna with square fractals, a leaf inspired Fern fractal Vivaldi antenna, a pentagon slots fractal antenna, a decagonal Sierpinski UWB Fractal antenna, a hybrid Moore's fractal antenna, a circular fractal antenna, etc. are proposed by the authors in [5–13]. MIMO fractal antennas with Koch fractals, Amer fractal slots, A Minkowski fractal shaped based isolator for isolation enhancement, an epsilon-shaped fractal UWB antenna, a compact fractal antenna, hexagonal slots fractal and double negative (DNG) metamaterial-based Koch fractal, high gain circular fractal UWB antenna for telecommunication applications are developed and presented in [14–22].

In this paper, a monopole fractal antenna is developed by inscribing hexagons and circles to obtain a wheel shaped hexa slots fractal structure with wide operating band. Section 2 describes a fractal antenna and a MIMO antenna development, their fabrication and operating bands. Section 3 discusses proposed MIMO antenna results such as S-parameter characteristics and far-filed radiation characteristics. MIMO antenna performance metrics and time domain behavior are presented in Section 4. The proposed antenna and other recent relevant works comparison is provided in Section 5. Conclusion of the proposed work by highlighting the investigations of MIMO antenna is depicted in Section 6.

2. ANTENNA DESIGN

A fractal monopole antenna for UWB applications with super wideband is presented in this paper. The proposed antenna design evolves from a simple circular microstrip patch antenna of dimensions $40 \times 45 \times 1.6\,\text{mm}^3$ with circular patch diameter of $d_1 = 25.2$ mm. It is designed on an FR-4 substrate of dielectric constant 4.4, and the bottom layer is partial ground plane. A hexagon of side $h_1 = 12.25$ mm is inscribed in it as represented in Figure 1(a). Then a circular patch of diameter $d_2 = 21.8$ mm is inscribed tangential to the side lengths of hexagon, and six slots are formed in the structure as presented in Figure 1(b) iteration-2. S_{11} characteristics of iteration-2 are presented in Figure 2. It achieved dual operating band from 1.63–9.35 GHz and 13.43–15.62 GHz. To further enhance the impedance bandwidth of the proposed antenna, fractal structure is designed by repeating the six slots five more times, and the structure appears as a fractal wheel shaped element with hexa

* Corresponding author: Usha Devi Yalavarthi (ushadevi.yalavarthi@kluniversity.in).

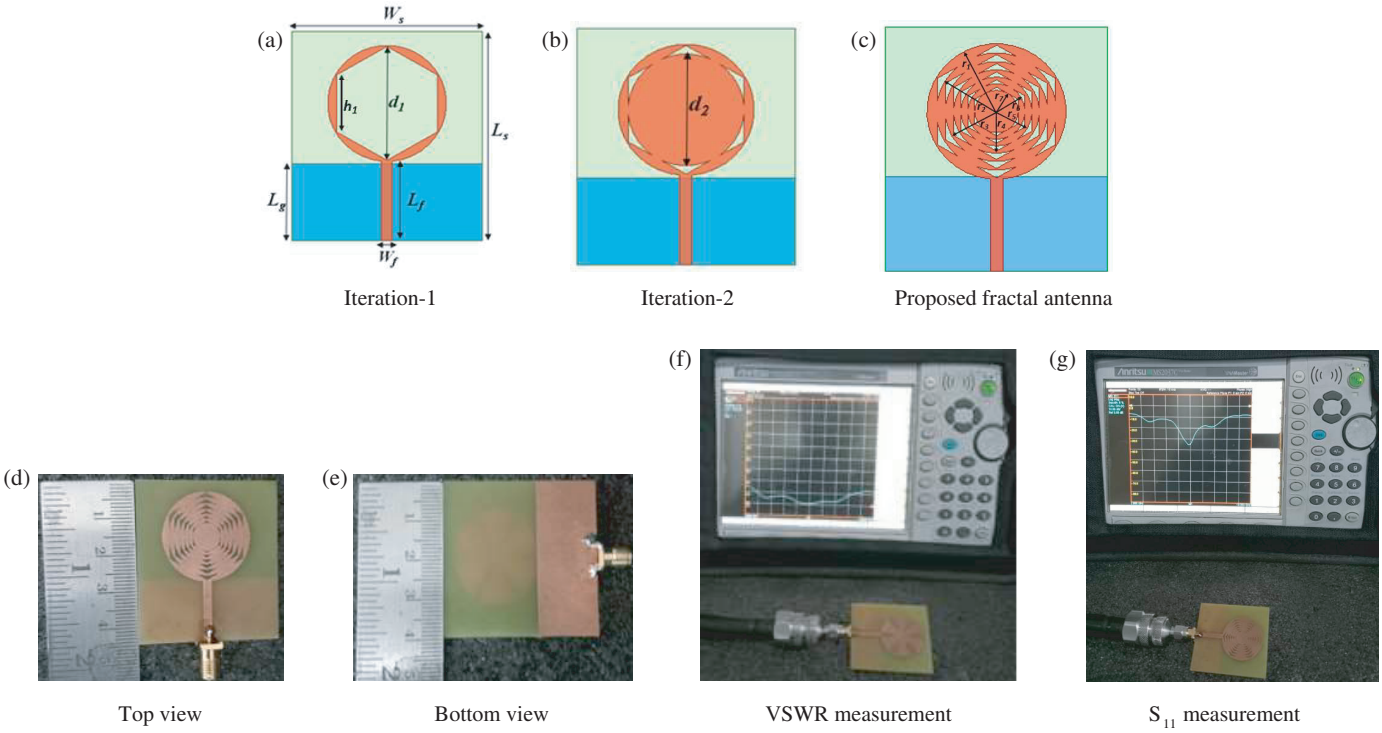

FIGURE 1. Proposed hexagon slot wheel shaped fractal antenna.

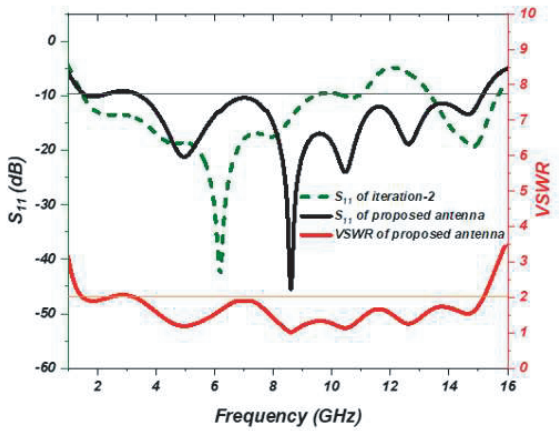

FIGURE 2. S_{11} and VSWR characteristics of proposed antenna.

TABLE 1. Dimensional specifications of proposed fractal antenna.

W_s	L_s	d_1	W_f	L_f	L_g	d_2	h_1	r_1	r_2	r_3	r_4	r_5	r_6	r_7
40	45	25.2	2.25	17.1	17.5	21.8	12.25	12.6	10.9	9.3	7.8	6.4	5.1	3.9

slots. The side of second inscribed hexagon is $h_2 = 10.5$ mm; that of the third inscribed hexagon is $h_3 = 8.85$ mm; that of the fourth inscribed hexagon is $h_4 = 7.3$ mm; that of the fifth inscribed hexagon is $h_5 = 5.85$ mm; and that of the sixth inscribed hexagon is $h_6 = 4.5$ mm. Fractal structure is obtained by maintaining a descending difference of 1.7, 1.6, 1.5, 1.4, 1.3, and 1.2 mm in radii between successive circles and 1.75, 1.65, 1.55, 1.45, and 1.35 mm between successive hexagon sides, respectively. Figure 1(c) depicts the proposed fractal wheel shaped antenna, and Table 1 gives the geometrical specifications of it in mm. Figures 1(d)–1(g) illustrate fabricated proposed antenna top view, bottom view, voltage standing wave ratio (VSWR) measurement, and S_{11} measurement on vector network analyzer (VNA).

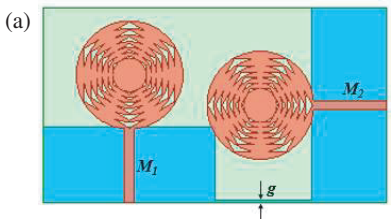

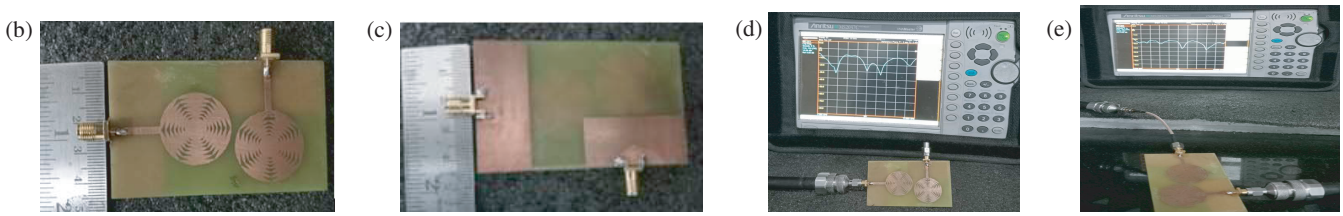

FIGURE 3. Proposed orthogonal MIMO fractal antenna.

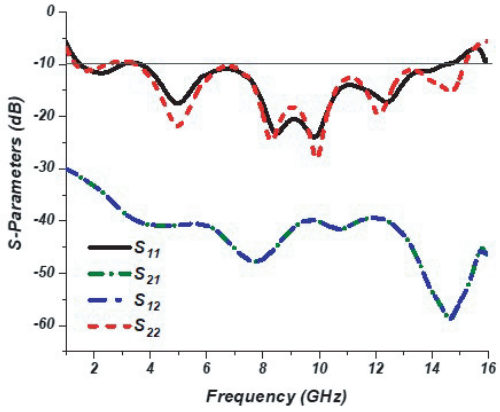

FIGURE 4. S-parameter characteristics.

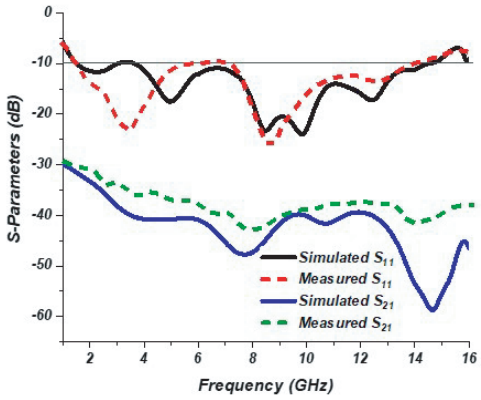

FIGURE 5. Port-1 S-parameters.

The proposed fractal antenna operates from 3.35 to 15.23 GHz with an impedance bandwidth ($S_{11} <= -10$ dB) of 11.88 GHz as illustrated in Figure 2. VSWR characteristics of the proposed antenna are represented in Figure 2. VSWR value lies between 2 and 1 from 3.25 GHz to 15.23 GHz. Therefore, the proposed fractal antenna matches well with transmission line and achieves higher efficiency.

Orthogonal MIMO antenna of the proposed fractal with polarization diversity is developed as illustrated in Figure 3(a). A fractal MIMO antenna with polarization diversity is significant in wireless communication as it enhances data throughput, improves signal reliability, mitigates interference, and offers spectrum efficiency. This technology is a valuable tool for ensuring robust and high-speed wireless communication in a wide range of applications. As represented in Figure 3(a), MIMO elements M_1 and M_2 are placed orthogonal to each other, and the ground planes are connected via $g = 0.5$ mm slot to overcome isolated ground problems. The MIMO antenna is fabricated on an FR-4 substrate of dimensions $80 \times 45 \times 1.6\,\text{mm}^3$, and prototyped antenna top view and bottom view are illustrated in Figures 3(b) and 3(c). It is tested for the validation with VNA experimentally, and far-field radiation characteristics are examined in an anechoic chamber. Reflection coefficient measurement and transmission coefficient measurement on VNA are presented in Figures 3(d) and 3(e), respectively.

3. RESULTS AND DISCUSSION

3.1. S-Parameters and VSWR Characteristics

Simulated S-parameter characteristics of the proposed MIMO antenna are depicted in Figure 4. From reflection coefficient characteristics S_{11} and S_{22} $<= -10$ dB, operating bands achieved are almost similar. An impedance bandwidth of 12.93 GHz from 1.58 to 14.51 GHz is obtained by M_1 element and M_2 element and operates from 1.39 to 15.18 GHz with an impedance bandwidth of 13.79 GHz. As antenna elements are identical, transmission coefficient characteristics S_{12} and S_{21} are identical and equal. They are represented in Figure 4 and $S_{12} = S_{21} < -32$ dB in the operating band. Therefore, the proposed MIMO antenna exhibits good isolation with simple ground structure and orthogonal placement of MIMO ele-

TABLE 2. S-parameters and VSWR values at different resonant frequencies.

Antenna	S_{11} (S_{22}) in dB			S_{21} (S_{12}) in dB			VSWR		
	5.8 GHz	8.3 GHz	10 GHz	5.8 GHz	8.3 GHz	10 GHz	5.8 GHz	8.3 GHz	10 GHz
Single	−15.14	−16.32	−18.61	-	-	-	1.42	1.19	1.26
M_1	−12.80	−22.11	−23.34	−40.62	−45.98	−40.11	1.61	1.17	1.15
M_2	−14.01	−25.13	−27.56	−40.62	−45.98	−40.11	1.50	1.11	1.09

TABLE 3. Peak gain and radiation efficiency values at different resonant frequencies.

Antenna	Peak Gain (dB)			Radiation Efficiency (%)		
	5.8 GHz	8.3 GHz	10 GHz	5.8 GHz	8.3 GHz	10 GHz
M_1	1.42	3.01	2.26	88.4	83.5	79.6
M_2	0.63	1.77	2.47	88.6	83.4	79.7

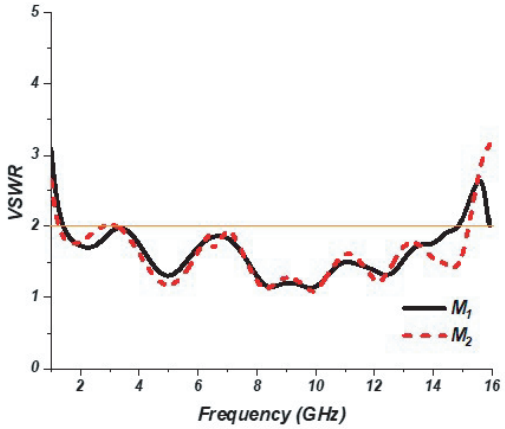

FIGURE 6. VSWR characteristics.

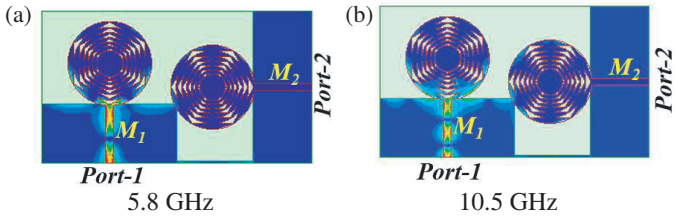

FIGURE 7. Surface current distribution of proposed MIMO antenna.

ments. Simulated and measured port-1 S-parameters of proposed MIMO antenna are described in Figure 5. S_{11} is similar in both cases with minute deviations, and measured S_{21} is less than −30 dB in the entire operating band. Hence, the proposed MIMO antenna elements have low mutual coupling.

Figure 6 illustrates VSWR characteristics of the proposed MIMO antenna. MIMO element M_1 attains good matching from 1.45 GHz to 14.86 GHz whereas element M_2 achieved good matching from 1.29 GHz to 15.23 GHz with minor deviations at 3 GHz (VSWR = 2.022). To examine the performance of proposed antenna, it is investigated at three different resonant frequencies: 5.8 GHz, 8.3 GHz, and 10 GHz. Table 2 gives S-parameter (reflection and transmission coefficients) and VSWR typical values at these frequencies.

3.2. Surface Current Distribution

Figure 7 gives the surface current distribution of proposed MIMO antenna at 5.8 GHz and 10.5 GHz resonant frequencies. For port-1 excitation, mutual coupling to port-2 is very little thereby maintaining better isolation between MIMO elements M_1 and M_2.

3.3. Far-Field Radiation Characteristics

3.3.1. Radiation Patterns

Measured radiation patterns of proposed single element fractal antenna and orthogonal MIMO antenna are illustrated in Figures 8(a), (b), (c), and (d) at 5.8 GHz and 10 GHz resonant frequencies. Radiation patterns are investigated for Theta = 90° and Phi = 90° planes, and the patterns are directive patterns.

3.3.2. Gain and Radiation Efficiency Characteristics

Peak gain vs frequency characteristics describe the peak gain achieved at each frequency step. As illustrated in Figure 9, the maximum gain attained by M_1 element is 3.62 dB at 13 GHz and 3.26 dB at 14.6 GHz by M_2 element. Simulated and measured gain values are in good agreement. Radiation efficiency characteristics of proposed MIMO antenna elements M_1 and M_2 are described in Figure 10. It varies from 96% to 68% in the operating band, and as frequency increases efficiency decreases. Typical values of peak gain in dB and radiation efficiency in % are tabulated in Table 3 for three resonant frequencies 5.8 GHz, 8.3 GHz, and 10 GHz.

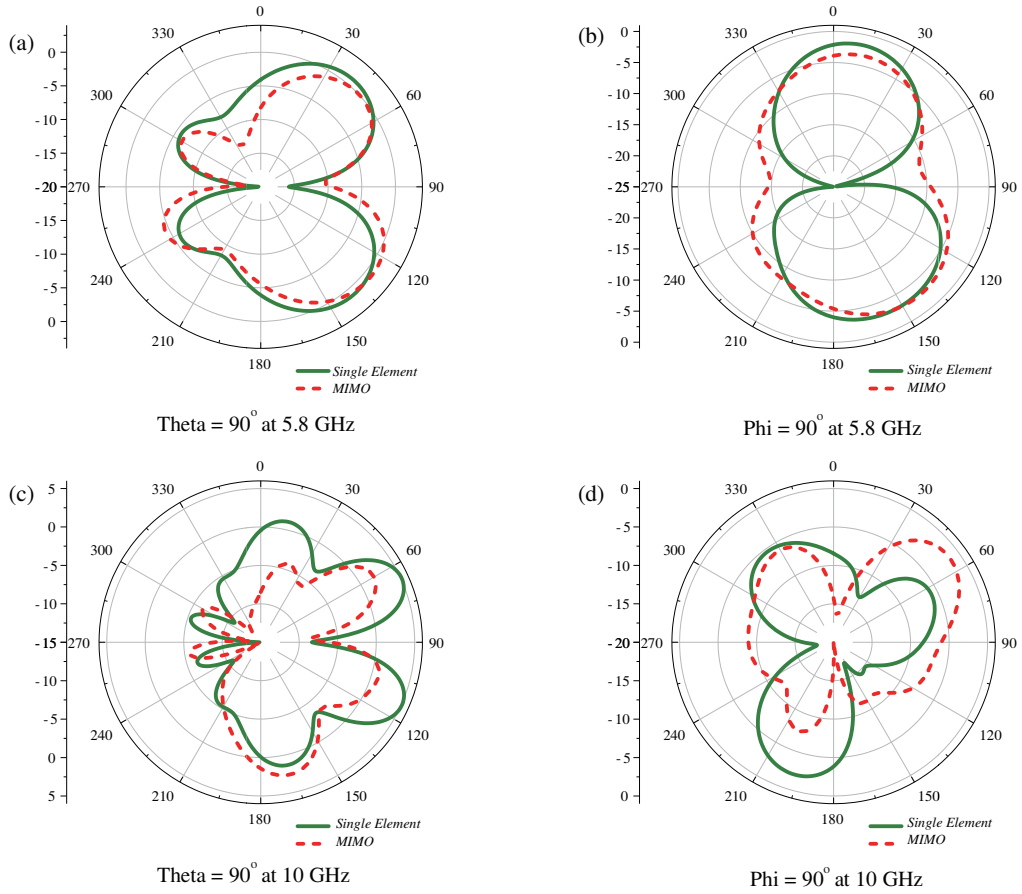

FIGURE 8. Radiations patterns in polar coordinates.

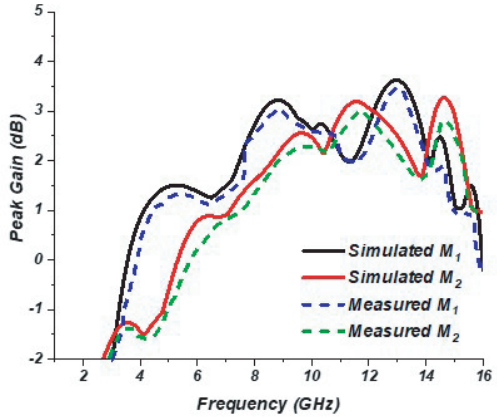

FIGURE 9. Peak gain characteristics.

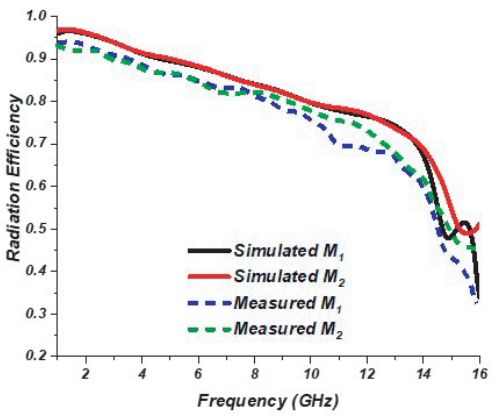

FIGURE 10. Radiation efficiency characteristics.

4. MIMO PERFORMANCE METRICS

4.1. Envelope Correlation Coefficient (ECC)

ECC characteristics of the proposed MIMO antenna are presented in Figure 11. ECC can be calculated from S-parameters or radiation patterns. However, if radiation efficiency is less than 97%, radiation patterns are preferable to avoid errors. Equation (1) is used to calculate ECC values from radiation patterns. From Figure 11, ECC of proposed antenna is less than 0.035 in the entire operating band. Therefore, proposed MIMO antenna has fine diversity performance with uncorrelated radiation patterns.

$$ECC = \frac{\left|\int_0^{2\pi}\int_0^{\pi}\left(XPRE_{\theta 1}E^*_{\theta 2}P_\theta + E_{\varphi_1}E^*_{\varphi 2}P_\varphi\right)d\Omega\right|^2}{\int_0^{2\pi}\int_0^{\pi}\left(XPRE_{\theta 1}E^*_{\theta 1}P_\theta + E_{\varphi_1}E^*_{\varphi 1}P_\varphi\right)d\Omega X \int_0^{2\pi}\int_0^{\pi}\left(XPRE_{\theta 2}E^*_{\theta 2}P_\theta + E_{\varphi 2}E^*_{\varphi 2}P_\varphi\right)d\Omega} \quad (1)$$

where $E_{\theta 1}$, $E_{\theta 2}$ are θ (vertical) polarized complex radiation patterns of M_1 and M_2, and E_{φ_1}, $E_{\varphi 2}$ are φ (horizontal) po-

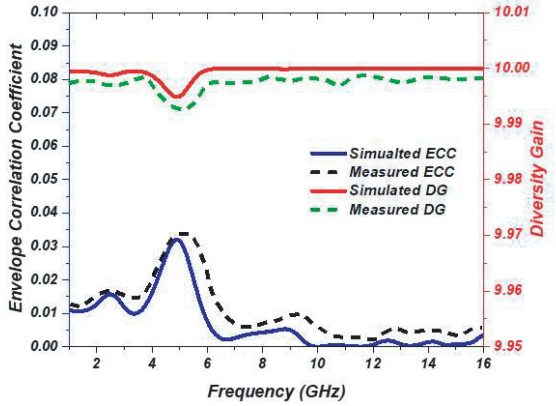

FIGURE 11. ECC and DG characteristics.

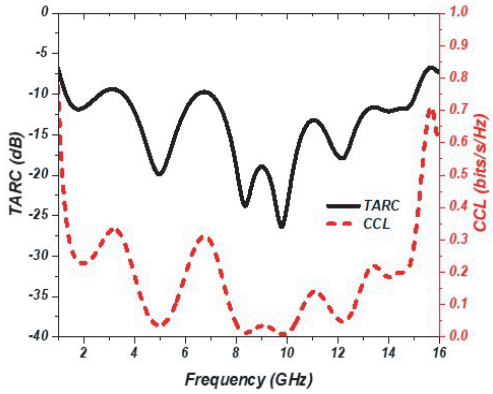

FIGURE 12. TARC and CCL characteristics.

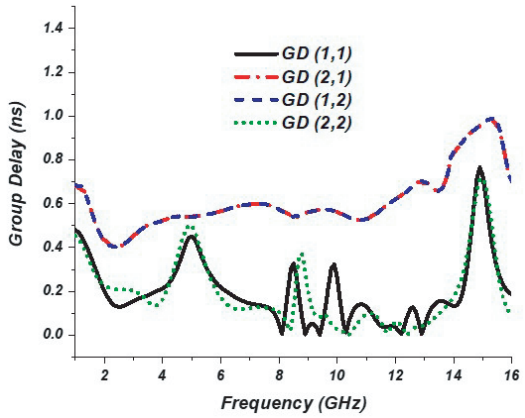

FIGURE 13. Group delay characteristics.

larized complex radiation patterns of M_1 and M_2. XPR is cross-polar discrimination, defined as time-averaged vertical-to-horizontal power ratio.

4.2. Diversity Gain (DG)

Figure 11 discusses DG characteristics, and DG values are very close to 10. Using Equation (2), diversity gain can be calculated from ECC values.

$$DG = 10\sqrt{1 - ECC^2} \tag{2}$$

4.3. Total Active Reflection Coefficient (TARC)

The effective operating bandwidth of MIMO antenna is defined by TARC characteristics. TRAC is obtained from S-parameters (two port network) as presented in Equation (3).

$$\Gamma_a^t = \sqrt{\frac{\left(\left(|s_{11} + s_{12}e^{j\theta}|^2\right) + \left(|s_{21} + S_{22}e^{j\theta}|^2\right)\right)}{2}} \tag{3}$$

where θ is the input feeding phase.

Figure 12 depicts TARC characteristics of the proposed MIMO antenna. It operates from 1.29 to 15.09 GHz with an effective operating bandwidth of 13.8 GHz.

4.4. Channel Capacity Loss (CCL)

The maximum limit for transmission without losses is given by CCL. For CCL $<$ 0.4 bits/s/Hz, lossless transmission is supported by MIMO antenna. Equations (4)–(7) are used to calculate CCL from S-parameters. Figure 12 illustrates CCL characteristics of the proposed MIMO antenna with respect to frequency. CCL values are less than 0.35 bits/s/Hz in the operating band.

$$\text{CCL} = -\log_2\left(\det\left(\psi^R\right)\right) \tag{4}$$

where,

$$\psi^R = \begin{bmatrix} \rho_{11} & \rho_{12} \\ \rho_{21} & \rho_{22} \end{bmatrix} \tag{5}$$

$$\rho_{ii} = 1 - \sum_{n=1}^{2} |S_{in}|^2 \tag{6}$$

$$\rho_{ij} = -\left(S_{ii}^* S_{ij} + S_{ji}^* S_{ij}\right) \tag{7}$$

Typical values of ECC, DG, TARC, and CCL of the proposed MIMO antenna at three resonant frequencies are presented in Table 4.

TABLE 4. ECC, DG, TARC and CCL values at different resonant frequencies.

Frequency (GHz)	ECC	DG	TARC (dB)	CCL (bits/s/Hz)
5.8	0.011	9.9993	−13.43	0.14
8.3	0.004	9.9998	−23.80	0.013
10	0.000003	10	−23.99	0.010

TABLE 5. Comparison of proposed MIMO antenna with other relevant works.

Reference	Dimensions (mm^3)	Operating Band (GHz)	Bandwidth (GHz)	Gain (dB)	Radiation Efficiency (%)	ECC	Isolation (dB)
[14]	$45 \times 45 \times 1.6$	2–10.6	8.6	4	-	< 0.005	> 17
[16]	$33 \times 33 \times 0.8$	1.5–19.2, 25–37.2	17.7, 12.2	1–6.3	50–85	< 0.05	> 25
[18]	$23.5 \times 35 \times 1$	1.78–30	28.22	6.6	85	< 0.1	> 22
[19]	$40 \times 40 \times 1.6$	5.62–6.16	0.54	-	-	< 0.005	> 30
This work	$40 \times 45 \times 1.6$	1.29–15.09	13.8	3.2	88.6	< 0.04	> 32

4.5. Group Delay

Group delay characterizes MIMO antenna time domain behavior. Measured group delay characteristics of proposed MIMO antenna (port-1 and port-2) are represented in Figure 13. Group Delay (GD) (m, n) denotes the delay from port m to port n. GDs (1,1), (2,1), (1,2), and (2,2) are illustrated in Figure 13. As M_1 and M_2 are identical and placed symmetrical, GD (1,2) = GD (2,1), and at all frequencies group delay is less than 1 ns. Therefore, the proposed MIMO antenna exhibits fine time domain behavior with minimum group delay.

5. COMPARISON

The proposed MIMO fractal antenna and other recent relevant works comparison is provided in Table 5. The parameters: dimensions of antenna, operating band, bandwidth, gain, radiation efficiency, ECC, and isolation are tabulated.

6. CONCLUSION

An orthogonal MIMO antenna with polarization diversity for UWB applications is presented in this paper. It consists of a hexa-slot wheel shaped fractal structure as radiating element and partial ground plane. The effective operating bandwidth (TARC) of proposed MIMO antenna is 13.8 GHz from 1.29 to 15.09 GHz. It achieved super wideband characteristics with good diversity performance. Isolation between MIMO elements is greater than 32 dB, and ECC is less than 0.04. Diversity gain is very close to 10, and CCL is less than 0.4 bits/s/Hz. 3.26 dB maximum peak gain is attained by it, and the average radiation efficiency is 83.11%. Therefore, the proposed MIMO antenna is suitable for UWB applications.

REFERENCES

[1] Oraizi, H. and S. Hedayati, "Miniaturized uwb monopole microstrip antenna design by the combination of giusepe peano and sierpinski carpet fractals," *IEEE Antennas and Wireless Propagation Letters*, Vol. 10, 67–70, 2011.

[2] Pourahmadazar, J., C. Ghobadi, and J. Nourinia, "Novel modified pythagorean tree fractal monopole antennas for UWB applications," *IEEE Antennas and Wireless Propagation Letters*, Vol. 10, 484–487, 2011.

[3] Li, D. and J.-F. Mao, "A Koch-like sided fractal bow-tie dipole antenna," *IEEE Transactions on Antennas and Propagation*, Vol. 60, No. 5, 2242–2251, May 2012.

[4] Naser-Moghadasi, M., R. A. Sadeghzadeh, T. Sedghi, T. Aribi, and B. S. Virdee, "UWB CPW-fed fractal patch antenna with band-notched function employing folded T-shaped element," *IEEE Antennas and Wireless Propagation Letters*, Vol. 12, 504–507, 2013.

[5] Kushwaha, N. and R. Kumar, "An UWB fractal antenna with defected ground structure and swastika shape electromagnetic band gap," *Progress In Electromagnetics Research B*, Vol. 52, 383–403, 2013.

[6] Amini, A., H. Oraizi, and M. A. C. Zadeh, "Miniaturized UWB log-periodic square fractal antenna," *IEEE Antennas and Wireless Propagation Letters*, Vol. 14, 1322–1325, 2015.

[7] Gorai, A., M. Pal, and R. Ghatak, "A compact fractal-shaped antenna for ultrawideband and bluetooth wireless systems with WLAN rejection functionality," *IEEE Antennas and Wireless Propagation Letters*, Vol. 16, 2163–2166, 2017.

[8] Biswas, B., R. Ghatak, and D. R. Poddar, "A fern fractal leaf inspired wideband antipodal Vivaldi antenna for microwave imaging system," *IEEE Transactions on Antennas and Propagation*, Vol. 65, No. 11, 6126–6129, Nov. 2017.

[9] Mohandoss, S., R. R. Thipparaju, B. N. B. Reddy, S. K. Palaniswamy, and P. Marudappa, "Fractal based ultra-wideband antenna development for wireless personal area communication applications," *AEU — International Journal of Electronics and Communications*, Vol. 93, 95–102, 2018.

[10] Ali, T., B. K. Subhash, and R. C. Biradar, "A miniaturized decagonal sierpinski UWB fractal antenna," *Progress In Electromagnetics Research C*, Vol. 84, 161–174, 2018.

[11] Khan, U. R., J. A. Sheikh, A. Junaid, R. Amin, S. Ashraf, and S. Ahmed, "Design of a compact hybrid Moore's fractal inspired wearable antenna for IoT enabled bio-telemetry in diagnostic health monitoring system," *IEEE Access*, Vol. 10, 116 129–116 140, 2022.

[12] Khan, M. A., U. Rafique, H. S. Savci, A. N. Nordin, S. H. Kiani, and S. M. Abbas, "Ultra-wideband pentagonal fractal antenna with stable radiation characteristics for microwave imaging applications," *Electronics*, Vol. 11, No. 13, 2061, Jul. 2022.

[13] Nejdi, I. H., S. Bri, M. Marzouk, S. Ahmad, Y. Rhazi, M. A. Lafkih, Y. A. Sheikh, A. Ghaffar, and M. Hussein, "UWB circular fractal antenna with high gain for telecommunication applications," *Sensors*, Vol. 23, No. 8, 4172, Apr. 2023.

[14] Tripathi, S., A. Mohan, and S. Yadav, "A compact Koch fractal UWB MIMO antenna with WLAN band-rejection," *IEEE Antennas and Wireless Propagation Letters*, Vol. 14, 1565–1568, 2015.

[15] Peristerianos, A., A. Theopoulos, A. G. Koutinos, T. Kaifas, and K. Siakavara, "Dual-band fractal semi-printed element antenna arrays for MIMO applications," *IEEE Antennas and Wireless Propagation Letters*, Vol. 15, 730–733, 2016.

[16] Debnath, P., A. Karmakar, A. Saha, and S. Huda, "UWB MIMO slot antenna with Minkowski fractal shaped isolators for isolation enhancement," *Progress In Electromagnetics Research M*, Vol. 75, 69–78, 2018.

[17] Abed, A. T. and A. M. Jawad, "Compact size MIMO Amer fractal slot antenna for 3G, LTE (4G), WLAN, WiMAX, ISM and 5G communications," *IEEE Access*, Vol. 7, 125 542–125 551, 2019.

[18] Chaudhary, A. K. and M. Manohar, "A modified SWB hexagonal fractal spatial diversity antenna with high isolation using meander line approach," *IEEE Access*, Vol. 10, 10 238–10 250, 2022.

[19] Sediq, H. T., J. Nourinia, C. Ghobadi, and B. Mohammadi, "An epsilon-shaped fractal antenna for UWB MIMO applications," *Applied Physics A — Materials Science & Processing*, Vol. 128, No. 9, 845, Sep. 2022.

[20] Punna, B. and P. Muthusamy, "Compact fractal based UWB MIMO antenna with dual band dispensation," *Analog Integrated Circuits and Signal Processing*, Vol. 112, No. 3, 485–494, Sep. 2022.

[21] Ez-Zaki, F., H. Belahrach, A. Ghammaz, S. Ahmad, A. Khabba, K. A. Belaid, A. Ghaffar, and M. I. Hussein, "Double negative (DNG) metamaterial-based Koch fractal MIMO antenna design for sub-6-GHz V2X communication," *IEEE Access*, Vol. 11, 77 620–77 635, 2023.

[22] Nejdi, I. H., S. Bri, M. Marzouk, S. Ahmad, Y. Rhazi, M. A. Lafkih, Y. A. Sheikh, A. Ghaffar, and M. Hussein, "UWB circular fractal antenna with high gain for telecommunication applications," *Sensors*, Vol. 23, No. 8, 4172, Apr. 2023.